

## The role of the solar irradiance variability in the evolution of the middle atmosphere during 2004–2009

A. V. Shapiro,<sup>1,2</sup> E. V. Rozanov,<sup>1,2</sup> A. I. Shapiro,<sup>1</sup> T. A. Egorova,<sup>1</sup> J. Harder,<sup>3</sup> M. Weber,<sup>4</sup> A. K. Smith,<sup>5</sup> W. Schmutz,<sup>1</sup> and T. Peter<sup>2</sup>

Received 2 August 2012; revised 18 December 2012; accepted 19 January 2013.

[1] Recent measurements by the Spectral Irradiance Monitor (SIM) and the Solar Stellar Irradiance Comparison Experiment (SOLSTICE) onboard the Solar Radiation and Climate Experiment satellite have revealed the spectral solar irradiance (SSI) changes in the ultraviolet between 2004 and 2009 to be several times higher than it was shown by all previous SSI measurements and reconstructions. In this paper, we simulate the O<sub>3</sub>, OH, and temperature responses to solar irradiance variability using four different SSI data sets trying to define which one gives the best agreement between the simulated and observed responses. First, we apply the 1-D radiative-convective model with interactive photochemistry to determine the regions of the atmosphere where the O<sub>3</sub>, OH, and temperature are most sensitive to the spectrum discrepancies between the different SSI data sets. As the comparison with observations can be only made taking into account dynamics and all known forcings of the atmosphere, we then apply the 3-D chemistry-climate model SOCOL to simulate the atmosphere evolution from May 2004 to February 2009. We compare the modeled OH, O<sub>3</sub>, and temperature changes with atmospheric data measured by several space instruments. Overall, the comparison shows that the atmospheric changes simulated with the 3-D SOCOL model driven by the SIM and SOLSTICE SSI are closest to the atmospheric measurements.

**Citation:** Shapiro, A. V., E. V. Rozanov, A. I. Shapiro, T. A. Egorova, J. Harder, M. Weber, A. K. Smith, W. Schmutz, and T. Peter (2013), The role of the solar irradiance variability in the evolution of the middle atmosphere during 2004–2009, *J. Geophys. Res. Atmos.*, 118, doi:10.1002/jgrd.50208.

### 1. Introduction

[2] UV solar radiation partly penetrates down to the middle atmosphere, triggering various photochemical and physical processes which influence atmospheric composition, dynamics, temperature, and structure [e.g., *Brasseur, 1993; Fleming et al., 1995; Rozanov et al., 2002; Egorova et al., 2005; Smith and Matthes, 2008; Tsutsui et al., 2009; Oberländer et al., 2012; Shapiro et al., 2012*].

[3] For the last few decades, spectral solar irradiance (SSI) was measured by a number of satellite instruments [e.g., *Brueckner et al., 1993; Thuillier et al., 2003; Pagaran*

*et al., 2011*] as well as reconstructed using different techniques [*Lean et al., 2005; Krivova et al., 2009; Shapiro et al., 2011a*]. In spite of the increased availability of observational data, the discrepancies between different measurements are not getting smaller. The data obtained by the Spectral Irradiance Monitor (SIM) and the Solar Stellar Irradiance Comparison Experiment instruments onboard the Solar Radiation and Climate Experiment (SORCE) satellite [*Rottman et al., 1993, 2005*] reveal that the UV variability during down branch of the 23rd solar cycle (2004–2009) can be several times higher in comparison with other SSI data and that the signs of the solar irradiance trends due to the 11 year activity are different in the visible and UV regions [*Harder et al., 2009*]. Moreover, the solar irradiance variability measured by the Spectral Irradiance Monitor (SIM) and the Solar Stellar Irradiance Comparison Experiment (SOLSTICE) is different in their common part of the spectrum (210–290 nm).

[4] The 210–290 spectral range covers the Herzberg continuum (200–242 nm) and the Hartley band (200–310 nm). The impact of the radiation in these spectral bands on photochemistry strongly affects the middle atmospheric state and composition. In particular, they influence the ozone concentration and temperature [e.g., *Brasseur, 1993; Rozanov et al., 2006*]. The comparison of the O<sub>3</sub> and temperature responses to the solar irradiance variability made using the different SSI data sets was under active

<sup>1</sup>Physical-Meteorological Observatory/World Radiation Center, Davos, Switzerland.

<sup>2</sup>Institute for Atmospheric and Climate Science ETH, Zurich, Switzerland.

<sup>3</sup>Laboratory for Atmospheric and Space Physics, Boulder, Colorado, USA.

<sup>4</sup>Institute of Environmental Physics, University of Bremen, Bremen, Germany.

<sup>5</sup>Atmospheric Chemistry Division, National Center for Atmospheric Research, Boulder, Colorado, USA.

Corresponding author: A. V. Shapiro, Physical-Meteorological Observatory/World Radiation Center, Davos, Switzerland. (anna.shapiro@pmodwrc.ch)

discussion for the last few years [e.g., *Cahalan et al.*, 2010; *Haigh et al.*, 2010; *Merkel et al.*, 2011; *Swartz et al.*, 2012]. These studies revealed a strong divergence between the responses obtained with the different SSI data sets. These investigations were made using idealized atmospheric conditions, as, for example, the analysis made by *Haigh et al.* [2010], which was based on 2-D model simulations. In other studies, 3-D models were used, but some important components of the atmospheric variability, such as quasi-biennial oscillation (QBO), chlorine trend, sea surface temperature (SST) changes, and greenhouse gas variability, were not taken into account. The exclusion of the dynamics and the atmospheric variability makes extracting of the solar signature from the modeled time series easier. However, if we want to compare our results with observations, we need to use the comprehensive 3-D models, including all possible forcings, in order to obtain a more realistic representation of the atmospheric evolution. This is especially important for the timescales that are comparable with the variability of the used forcings.

[5] In this paper, we study the atmospheric response to solar irradiance variability using four different SSI data sets (SIM, SOLSTICE-based composites, *Lean et al.* [2005] reconstruction, and constant solar forcing). First we apply a 1-D chemistry-climate model (CCM) to understand which photochemical mechanisms are responsible for the divergence in the OH, O<sub>3</sub>, and temperature atmospheric responses calculated with the different SSI data sets and determine heights where this divergence is the strongest. To compare with observations, we then simulate the atmospheric evolution using the 3-D chemistry-climate model SOCOL that takes into account QBO, chlorine trend, sea surface temperature changes, and greenhouse gas variability.

[6] In section 2, we describe the data used for our analysis. We present the results of the 1-D modeling in section 3 and of the 3-D modeling results in section 4. The comparison with atmospheric measurements is shown in section 5. We summarize our conclusions in section 6.

## 2. Description of the Applied Data Sets

### 2.1. SSI Data Sets

[7] For our analysis, we used four SSI data sets: two measured, one theoretical, and one reference. We term the data sets as follows:

1. “NO SUN”: SSI was kept constant to values corresponding to January 2004.
2. “NRL”: SSI reconstructed by *Lean et al.* [2005].
3. “SIM”: composite which contains the SORCE SOLSTICE data from 121 to 210 nm and the SIM data from 210 to 750 nm.
4. “SOLSTICE”: composite which contains the SORCE SOLSTICE data from 121 to 290 nm and the SIM data from 290 to 750 nm.

[8] We analyze the data for the period from May 2004 to February 2009 as the shortwave (210–310 nm) SIM data are only available for this period of time. We used the SOLSTICE data up to 290 nm and the SIM data from 210 nm according to the recommendations of the SORCE team.

[9] Two of the used data sets are based on measurements of the solar irradiance by the SIM and SOLSTICE instruments onboard the SORCE satellite, which was launched on 25 January 2003. The SOLSTICE instrument, which is a follow-up to the SOLSTICE onboard Upper Atmospheric Research Satellite (UARS) launched in 1991 [*Rottman et al.*, 1993], measures the daily spectral irradiance with absolute accuracy of 5% and with relative accuracy of 0.5% per year in the spectral range from 115 to 320 nm [*McClintock et al.*, 2005]. The SIM instrument is a newly designed spectrometer that measures the irradiance in the visible and near-infrared from 300 to 1600 nm with an additional UV channel (200–300 nm) that overlaps with the SOLSTICE irradiance measurements [*Harder et al.*, 2000]. In this paper, we used the reported SIM irradiance in the visible range. The absolute accuracy of the SIM instrument at visible wavelengths is about 2%. The relative accuracy is about 300 ppm (1 $\sigma$ ) for wavelengths greater than 500 nm. It decreases to shorter wavelengths and reaches approximately 0.5% at 310 nm and is then signal-to-noise limited at 220 nm to about 1%. To provide redundancy and self-calibration capability, SIM contains two completely independent and identical (mirror-image) spectrometers; the relative accuracy is based on detailed comparisons of these two spectrometers during the April 2004 to November 2007 (3.45 years) time frame and are valid through the time period considered in this paper and are consistent with the values quoted in *Harder et al.* [2009]. A detailed description of the SIM instrument was published by *Harder et al.* [2005a, 2005b], and the measurement equations for the degradation corrections are presented in the Auxiliary Materials section in *Harder et al.* [2009].

[10] The SSI reconstruction by *Lean et al.* [2005] is based on different proxies of the solar activity. It employs the sunspot area records to represent the sunspot darkening and Mg II, Ca II, and f10.7 indices to represent the facular brightening [*Lean*, 1997; *Lean*, 2000; *Ermolli et al.*, 2012]. Below 400 nm, the contrast is calculated by employing UARS/SOLSTICE observations, while above 400 nm, they are based on the model by *Solanki and Unruh* [1998]. The reconstruction covers the spectral range 120 nm to 100  $\mu$ m.

[11] The NRL, SIM, and SOLSTICE SSI changes between May 2004 and February 2009 at 120–450 nm are presented in Figure 1. In the 200–350 nm range, the variability measured by SOLSTICE and SIM is significantly stronger than the variability yielded by the NRL model. At the same

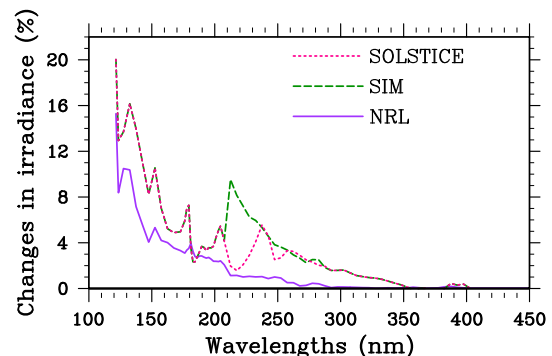


**Figure 1.** The SSI relative changes between May 2004 and February 2009 for the SIM, SOLSTICE, and NRL data.

time, the SIM and SOLSTICE SSI variabilities are also different in the range where their spectra overlap. The SSI measured by SIM is more variable than the SSI measured by SOLSTICE at 210–235 nm. At this interval, the SIM data have a lower signal-to-noise ratio than the data measured by the SOLSTICE instrument. These discrepancies between the different SSI data sets influence photolysis rates and, as a result, influence atmospheric chemistry and temperature [Brasseur and Solomon, 2005].

## 2.2. Atmospheric Measurements

[12] For atmospheric constituents, we used the data obtained by three instruments.

[13] Sounding of the Atmosphere using Broadband Emission Radiometry (SABER) instrument [Russell *et al.*, 1999] onboard the Thermosphere, Ionosphere, Mesosphere, Energetic and Dynamics (TIMED) spacecraft that was launched in December 2001. It scans the atmospheric limb and measures the emitted infrared radiation at some spectral bands. For this analysis, we used 2 months averaged O<sub>3</sub> and temperature profiles from version 1.07. As August SABER data, we used the data averaged over August and September.

[14] Scanning Imaging Absorption Spectrometer for Atmospheric Cartography (SCIAMACHY) instrument [Burrows *et al.*, 1995; Bovensmann *et al.*, 1999] onboard the Environmental Satellite (Envisat) spacecraft that was launched on 1 March 2002 into a Sun synchronous polar orbit. The mission formally ended on 9 May 2012. SCIAMACHY is a spectrometer that was designed to measure scattered, reflected, or transmitted sunlight. In our study, we use O<sub>3</sub> profiles from version 2.5.

[15] Microwave Limb Sounder (MLS) instrument onboard the Aura satellite. Aura was launched on 15 July 2004 on a Sun synchronous near-polar orbit. MLS observes the thermal emission from the Earth's limb in spectral intervals with centers at 118 GHz, 190 GHz, 240 GHz, 640 GHz, and 2.5 THz [Waters *et al.*, 2006]. In this work, we use version 3.3 for O<sub>3</sub> and temperature [Livesey *et al.*, 2011].

[16] Solar Backscatter Ultraviolet Radiometer (SBUV) is a family of nadir-oriented instruments on NOAA weather satellites [Heath *et al.*, 1975]. SBUV measures the UV irradiance scattered by the Earth's atmosphere. This allows monitoring the concentration and vertical distribution of atmospheric ozone. In this paper, we used the data obtained by NOAA-17, which operated from 2002 to 2010 and measured the irradiance in the 160–406 nm spectral range.

[17] In addition, for the comparison of dynamical influences, we use ERA INTERIM [Dee *et al.*, 2011], which is one of the three and the latest global atmospheric reanalysis produced by the European Centre for Medium-Range Weather Forecast. The data are based on the observations by the different instruments (e.g., radiosondes, balloons, aircraft, and satellites). It extends from 1979 to the present and describes the state of the atmosphere, land, and ocean-wave conditions.

## 3. 1-D Modeling

### 3.1. Model Description and Experimental Setup

[18] The 1-D radiative-convective model with interactive neutral and ion chemistry (RCMC) is applied in our study. The model was developed by Egorova *et al.* [1997] and Rozanov *et al.* [2002]. It is coupled to the ion chemistry

module described by Ozolin *et al.* [2009]. The model consists of the radiation, chemistry, convective adjustment, and vertical diffusion modules. The atmosphere is divided into 40 layers that extend from the ground to 100 km. The input solar spectrum covers the wavelength range from 121 to 750 nm and is divided into 73 intervals. The model computes the temperature profile and the distribution of 43 neutral chemical species of the oxygen, nitrogen, hydrogen, carbon, chlorine, and bromine groups and 48 ions (31 positive and 17 negative). The chemical solver utilizes the implicit iterative Newton-Raphson scheme [Rozanov *et al.*, 1999]. The reaction coefficients are taken from Sander *et al.* [2006] for neutral atmospheric components and from Kopp [1996] and Kazil [2002] for ionized species in the ionosphere. The convective adjustment is treated according to Egorova *et al.* [1997]. The vertical turbulent transport of long-lived species was calculated using typical annual mean values of the eddy diffusion coefficients. The radiation scheme of Fomichev *et al.* [1998] was applied to treat mesospheric nonlocal thermodynamic equilibrium processes.

[19] In our study, we applied the 1-D model to tropical atmosphere. The SIM, SOLSTICE, and NRL SSI data sets described in section 2.1 were used to calculate the photolysis and heating rates which force the model. All runs were executed for 50 years. Repeated monthly SSI for November 2004 and November 2007 was used for the simulations. All experiments started from the same initial atmospheric conditions.

### 3.2. Results

[20] The OH, O<sub>3</sub>, and temperature responses to the different solar variabilities calculated as a difference between November 2004 and November 2007 values are presented in Figure 2. We will refer to the responses as OH, O<sub>3</sub>, or temperature-SSI data sets. The OH, O<sub>3</sub>, and temperature responses increase from 20 to 40 km. O<sub>3</sub>-SIM grows stronger than O<sub>3</sub>-SOLSTICE and O<sub>3</sub>-NRL at these heights (Figure 2b). At about 38 km, O<sub>3</sub>-SIM has its local maximum. Higher up to 50 km, the OH and temperature responses (Figures 2a and 2c) still grow, while the O<sub>3</sub> responses start to decrease. O<sub>3</sub>-SIM and O<sub>3</sub>-NRL are equal at about 50 km. The O<sub>3</sub> responses decrease from 50 to 70 km. At about 70 km, they have their minimum. From 70 to 80 km, the O<sub>3</sub> responses grow. In contrary to this, the OH responses have their maximum at about 70 km and decrease from 70 to 80 km. The temperature responses have the local maximum at about 50 km. Higher up to 70 km, the responses fall and grow again up to 80 km. Temperature-SIM and temperature-SOLSTICE are especially strong. O<sub>3</sub>-NRL is in good agreement with the results obtained by Haigh *et al.* [2010]. O<sub>3</sub>-SIM is similar to the results by Haigh *et al.* [2010] up to 40 km, but higher, the response calculated by Haigh *et al.* [2010] is smaller than the one obtained by our model.

[21] To estimate the influence of the particular spectral intervals on the atmospheric response, we performed a few additional experiments with the SSI data. During each experiment, we drive the model with SSI that changes only in some specific spectral regions, while the SSI in the other part of the spectrum is kept constant.

[22] In our first experiment, we drive the model allowing SSI changes only in the 121–200 nm spectral range. It covers the Ly- $\alpha$  line (121.6 nm) and Schumann-Runge bands (175–200 nm). As both SIM and SOLSTICE data

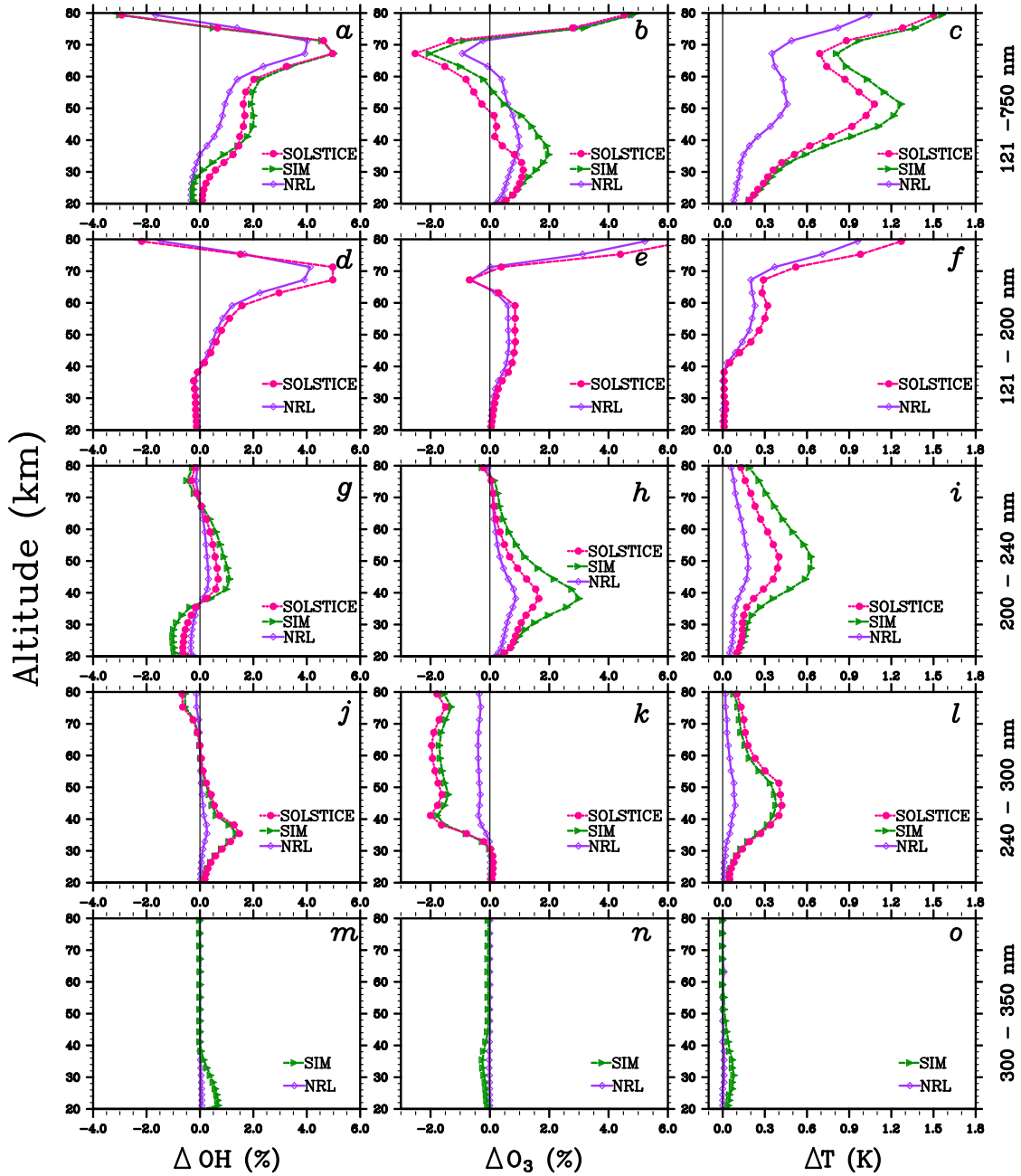


**Figure 2.** The (left) OH, (middle)  $\text{O}_3$ , and (right) temperature responses obtained with the SIM, SOLSTICE, and NRL data between November 2004 and November 2007. The responses were calculated for the variability at (a–c) 121–750 nm, (d–f) 121–200 nm, (g–i) 200–240 nm, (j–l) 240–300 nm, and (m–o) 300–350 nm spectral bands.

contain the SOLSTICE irradiance at wavelengths shorter than 200 nm, we analyze the atmospheric responses obtained with the SOLSTICE and NRL data. At 20–40 km, OH,  $\text{O}_3$ , and temperature (Figures 2d–2f) do not show any sensitivity to the considered spectral range, although in the main experiment (121–750 nm), there is a response at these heights. Thus, we can conclude that the radiation at 121–200 nm does not penetrate below 40 km. At higher altitudes (40–70 km), the enhancement of the radiation at 121–200 nm forces the water vapor photolysis ( $\text{H}_2\text{O} + h\nu \rightarrow \text{H} + \text{OH}$  for  $\lambda \leq 200$  nm) and, hence, the OH production. As the SOLSTICE data at 121–200 nm is more variable than the NRL

irradiance, OH-SOLSTICE is larger than OH-NRL. At about 70 km, the OH responses obtained during this experiment are equal to the OH responses calculated in the main experiment. Then, we can conclude that the OH changes at this height are forced by the irradiance variability at 121–200 nm. The increase of OH strengthens  $\text{HO}_x$  catalytic cycles and, as a result, accelerates the  $\text{O}_3$  destruction. In opposite, the  $\text{O}_2$  photolysis ( $\text{O}_2 + h\nu \rightarrow 2\text{O}$  for  $\lambda \leq 242.4$  nm) leads to the  $\text{O}_3$  production. Thus, on the one hand, the high SOLSTICE irradiance variability leads to the larger  $\text{O}_3$  loss by the water vapor photolysis, but on the other hand, it also influences the  $\text{O}_3$  production by the  $\text{O}_2$  photolysis. At 40–60 and about

80 km, the O<sub>3</sub> production dominates the destruction, and the larger SOLSTICE variability at 121–200 nm leads to larger O<sub>3</sub>–SOLSTICE in comparison with O<sub>3</sub>–NRL. Both O<sub>2</sub> and O<sub>3</sub> photolysis heat the atmosphere (Figure 2f), and the temperature changes are positive. Temperature–SOLSTICE is larger than temperature–NRL due to the higher variability of the SOLSTICE SSI. It was shown by Shapiro *et al.* [2011b] that the Ly- $\alpha$  line irradiance does not influence the layers below 60 km. Thus, we can conclude that the OH, O<sub>3</sub>, and temperature changes at 40–60 km shown in Figures 2d–2f are forced by the variability at 122–200 nm.

[23] In our second experiment, we considered the influence of the 200–240 nm spectral range on the middle atmospheric response. For this purpose, we forced the model by the solar variability at 200–240 nm, while the irradiance at 121–200 and 240–750 nm was kept constant. As one can see from Figure 1, the strongest disagreement between the SSI data sets is in the Herzberg continuum (200–242 nm), which also overlaps with part of the Hartley band (200–310 nm). While the irradiance at the Herzberg continuum forces the O<sub>3</sub> production, the Hartley band irradiance enchantment leads to the O<sub>3</sub> destruction by O<sub>3</sub> photolysis ( $O_3 + h\nu \rightarrow O_2 + O(^1D)$ ). The O<sub>3</sub> responses obtained in this experiment are positive at 20–80 km. Thus, we can conclude that the O<sub>3</sub> production dominates the destruction at these heights. The maximum of the O<sub>3</sub> response is at about 40 km. Both O<sub>2</sub> and O<sub>3</sub> photolysis lead to the atomic oxygen production. As a result of the photolysis, the temperature increases within the 20–70 km altitude range (Figure 2i), while the atomic oxygen production leads to an increase of the OH concentration via reaction  $O(^1D) + H_2O \rightarrow 2OH$  (Figure 2g) at the 35–70 km altitude range. The OH and temperature maximum positive responses are at about 45 km. Below 40 km, the photolysis role is weakening. This leads to the decrease of the O<sub>3</sub> and temperature responses. The OH response becomes negative as the OH production cannot compensate the OH destruction (e.g., by methane oxidation  $CH_4 + OH \rightarrow CH_3 + H_2O$ ). The SIM data are the most variable at the 200–240 nm range. As a result, the OH, O<sub>3</sub>, and temperature responses calculated with the SIM data are larger than the responses calculated with NRL and SOLSTICE data sets.

[24] The influence of the 240–300 nm spectral range on the middle atmospheric is analyzed during our third experiment. The radiation at these wavelengths cannot trigger the O<sub>2</sub> photolysis, while the O<sub>3</sub> photolysis can be easily forced by this irradiance. The absence of the O<sub>3</sub> production by O<sub>2</sub> photolysis and the O<sub>3</sub> destruction by the O<sub>3</sub> photolysis lead to the negative O<sub>3</sub> response at 20–80 km (Figure 2k). The O<sub>3</sub> photolysis forces the OH production ( $O(^1D) + H_2O \rightarrow 2OH$ ) as well as NO<sub>x</sub> and ClO<sub>x</sub> production by the production O(^1D). Therefore, the OH response is positive at 20–60 km and has a maximum at about 35 km (Figure 2j). The heating of the middle atmosphere by the O<sub>3</sub> photolysis leads to the positive temperature response at 20–80 km (Figure 2l). From 40 to 20 km, the OH, O<sub>3</sub>, and temperature responses are weakening. This can be explained by substantial absorption of 240–300 nm radiation at these altitudes. The SOLSTICE and SIM irradiance difference is not large for this spectral range as the difference between these two data sets and the NRL data. As a result, the responses obtained with SIM and

SOLSTICE data are similar and stronger than the responses calculated using the NRL time series.

[25] The last experiment is performed for the Huggins bands (300–350 nm). Both SIM and SOLSTICE composites contain the Huggins bands from the SIM data. Thus, we compare the responses obtained with the SIM and NRL SSI. The Huggins band irradiance is responsible for the O<sub>3</sub> destruction by  $O_3 + h\nu \rightarrow O_2 + O(^3P)$  for  $\lambda \geq 320$  nm or  $O_3 + h\nu \rightarrow O_2 + O(^1D)$  for  $\lambda \leq 320$  nm. As it was shown in our previous experiment, the O<sub>3</sub> photolysis leads to the negative O<sub>3</sub> response (Figure 2n), while the OH (Figure 2m) and temperature (Figure 2o) responses forced by the O<sub>3</sub> photolysis are positive. The SIM variability at this spectral band is substantially larger than the NRL variability (Figure 1). Thus, OH and temperature responses obtained with SIM SSI are larger than the ones calculated with the NRL irradiance. O<sub>3</sub>–SIM is smaller than O<sub>3</sub>–NRL. It should be noticed that all responses obtained during this experiment are very weak at 20–45 km and negligible at 45–80 km.

[26] We do not present the influence of the 350–750 nm spectral range on the middle atmosphere because one can see that the sum of the responses obtained during all four experiments is similar to the value of the corresponding responses calculated in the main experiment. Thus, we can conclude that the irradiance at 350–750 nm does not strongly influence the middle atmosphere.

## 4. The 3-D Modeling

### 4.1. Model Description and Experimental Setup

[27] The chemistry-climate model SOCOL is a combination of General Circulation Model MAECHAM4 [Manzini and Bengtsson, 1996] and the atmospheric chemistry transport model MEZON [Rozanov *et al.*, 1999, 2001; Egorova *et al.*, 2003]. It is a spectral general circulation model with T30 horizontal truncation. SOCOL has 39 vertical layers that cover the atmosphere from the surface to 0.01 hPa (about 80 km) altitude. The input solar spectrum is from 121 to 750 nm. The photolysis rates are calculated every 2 h, but heating and cooling rates are obtained every 15 min. The MEZON part simulates 41 chemistry species from the oxygen, hydrogen, nitrogen, chlorine, and bromine groups. In addition, 16 heterogeneous reactions on/in surface aerosol and polar stratospheric cloud particles are taken into account. The chemical solver is based on the pure implicit iterative Newton-Raphson scheme. For the chemical species calculations, the time-dependent CO<sub>2</sub>, CH<sub>4</sub>, N<sub>2</sub>O, and ODS mixing ratios are prescribed. SST and sea ice distribution were prescribed according to Rayner *et al.* [2003] with a monthly resolution. The horizontal and vertical winds, temperature, and humidity in the troposphere are calculated in the MAECHAM4 part for the MEZON part, while the MEZON part calculates the 3-D fields of O<sub>3</sub> and stratospheric H<sub>2</sub>O for the net radiative heating MAECHAM4 calculations. The Singapore measurements of zonal wind profiles were used to nudge the QBO according to Giorgetta [1996].

[28] For this study, the four SSI data sets described in section 2.1 were used to calculate the monthly photolysis rates from January 2004 to February 2009. The NO SUN rates were obtained using repeated January 2004 SSI. The monthly data observed by the SIM instrument are only available from

May 2004. Therefore, both SIM and SOLSTICE composites used in this study are based on the SIM and SOLSTICE SSI correspondingly from May 2004. To prolong these composites to January 2004, we based the SOLSTICE and SIM composites for January–April 2004 on the NRL SSI data. To avoid any shifts in the simulated time series, the latter were scaled to the SIM (SOLSTICE) data for May 2004. The SSI data are usually normalized to one astronomical unit. As the aim of this work is comparison of the modeled results with atmospheric measurements, we renormalized the data back to the normal orbital parameters.

[29] We carried out an ensemble of five transient runs for each data set. The ensemble members were started with a slightly different initial  $\text{CO}_2$  concentration.

[30] In this study, we consider the simulated middle atmosphere evolution of the tropical mean ( $18^\circ\text{N}$ – $18^\circ\text{S}$ ) OH,  $\text{O}_3$ , and temperature from May 2004 to February 2009.

## 4.2. Results

[31] As described in section 3.2, the 200–240 nm spectral interval variability is very important for the OH,  $\text{O}_3$ , and temperature changes in the stratosphere. In our analysis, we use the irradiance at 230 nm as a proxy for the solar variability. The 230 nm irradiance is chosen because it belongs to the two important for the middle atmosphere spectral ranges: Herzberg continuum and Hartley band. The influence of the ranges on the middle atmosphere was broadly discussed in section 3.2. We calculate the irradiance anomalies, which are deviations from the mean value over the period from May 2004 to February 2009, for SIM, SOLSTICE, and NRL irradiance at 230 nm (Figure 3). One can see that the NRL irradiance shows the weakest variability (about 1%), while the SIM and SOLSTICE data are more variable. The variability as measured by SIM reaches approximately 7%, while the variability yielded by SOLSTICE is about 5%.

[32] The NO SUN data contain all atmospheric variability, except the variability forced by the solar activity. Then using the multiple regression analysis, we can extract the solar signatures from the time series simulated with the NRL, SOLSTICE, and SIM SSI to estimate the pure effect of the SSI variability on the atmospheric response. Our regression model is as follows:

$$Y(t) = a + b * x_1(t) + c * x_2(t)$$

where  $t$  is time;  $x_1(t)$  is the irradiance at 230 nm;  $x_2(t)$  is OH,  $\text{O}_3$ , or temperature obtained from the NO SUN run; and  $Y(t)$  is OH,  $\text{O}_3$ , and temperature calculated with the different SSI data sets. We consider the period from May 2004 to February 2009.

[33] According to the results obtained with the 1-D model and discussed in section 3.2, the strong middle atmospheric response can be found at about 41 (3 hPa), 46 (1.5 hPa), and 70 (0.05 hPa) km altitude. Thus, we analyze the OH,  $\text{O}_3$ , or temperature solar signatures ( $b * x_1(t)$ ) calculated as ensemble means for these heights. Although the response at 70 km is mostly forced by the variability at the Ly- $\alpha$  line, the correlation between the Ly- $\alpha$  line and the 230 nm irradiance measured by the SOLSTICE instrument is high, and we can use the irradiance at 230 nm as a proxy at 70 km.

[34] The OH,  $\text{O}_3$ , or temperature solar signatures with  $1\sigma$  deviations are presented in Figure 4. As discussed in section 3.2, the OH production,  $\text{O}_3$  destruction, and temperature enhancement at  $\approx 70$  km is mostly forced by the  $\text{H}_2\text{O}$  photolysis, which is driven by the Ly- $\alpha$  line irradiance. Both used SIM and SOLSTICE composites contain the SOLSTICE Ly- $\alpha$  line irradiance, whose variability is different from the NRL Ly- $\alpha$  line irradiance variability (Figure 1). In agreement with 1-D-modeled results (Figures 2a and 2b), there is the difference between the OH responses obtained with the different SSI (Figure 4a), while the  $\text{O}_3$  responses are similar at these heights (Figure 4d). The signs of the obtained OH and  $\text{O}_3$  responses are consistent with the 1-D-modeled results presented in Figures 2a and 2b. The  $1\sigma$  deviations calculated for the temperature responses are so large that one cannot clearly define the differences between the responses obtained with different SSI as well as compare the obtained results with 1-D model simulations.

[35] In agreement with the 1-D-modeled results (Figures 2a–2c), the OH and temperature solar signatures at  $\approx 41$  and  $\approx 46$  km are in phase with the solar irradiance variability (Figures 4b, 4c, 4h, and 4i), as well as the  $\text{O}_3$  solar signatures at  $\approx 41$  km due to the  $\text{O}_2$  photolysis that dominates the  $\text{O}_3$  photolysis at these heights. Besides, at 41 and  $\approx 46$  km, the 1-D-modeled SIM and SOLSTICE OH responses are different from OH-NRL (Figure 2a). The 3-D-modeled solar signatures show similar behavior (Figures 4b and 4c). The large  $1\sigma$  deviations obtained for the temperature time series do not allow us to confidently estimate the differences between the temperature responses calculated with the different SSI.

[36] The crossing point of the NRL and SOLSTICE  $\text{O}_3$  responses calculated with the 1-D model is at  $\approx 38$  km, while  $\text{O}_3$ -SIM at this height is larger than the NRL and SOLSTICE responses. Higher  $\text{O}_3$ -SOLSTICE obtained with the 1-D model is smaller than  $\text{O}_3$ -SIM and  $\text{O}_3$ -NRL and, at about 50 km, becomes negative. The  $\text{O}_3$  solar signatures calculated with the 3-D model at  $\approx 41$  km show similar behavior to the 1-D-modeled responses at about 35 km (Figure 4f). At 46 km, 3-D- and 1-D-modeled  $\text{O}_3$  solar responses can be qualified as similar.

[37] At some heights, the  $1\sigma$  deviations calculated for the responses are so large that we cannot confidently distinguish the differences between the responses. However, one can see that the 1-D- and 3-D-modeled responses are overall in

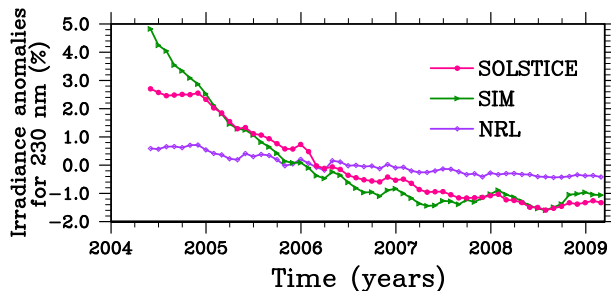


**Figure 3.** The SSI anomalies for 230 nm calculated with the SIM, SOLSTICE, and NRL data from May 2004 to February 2009.

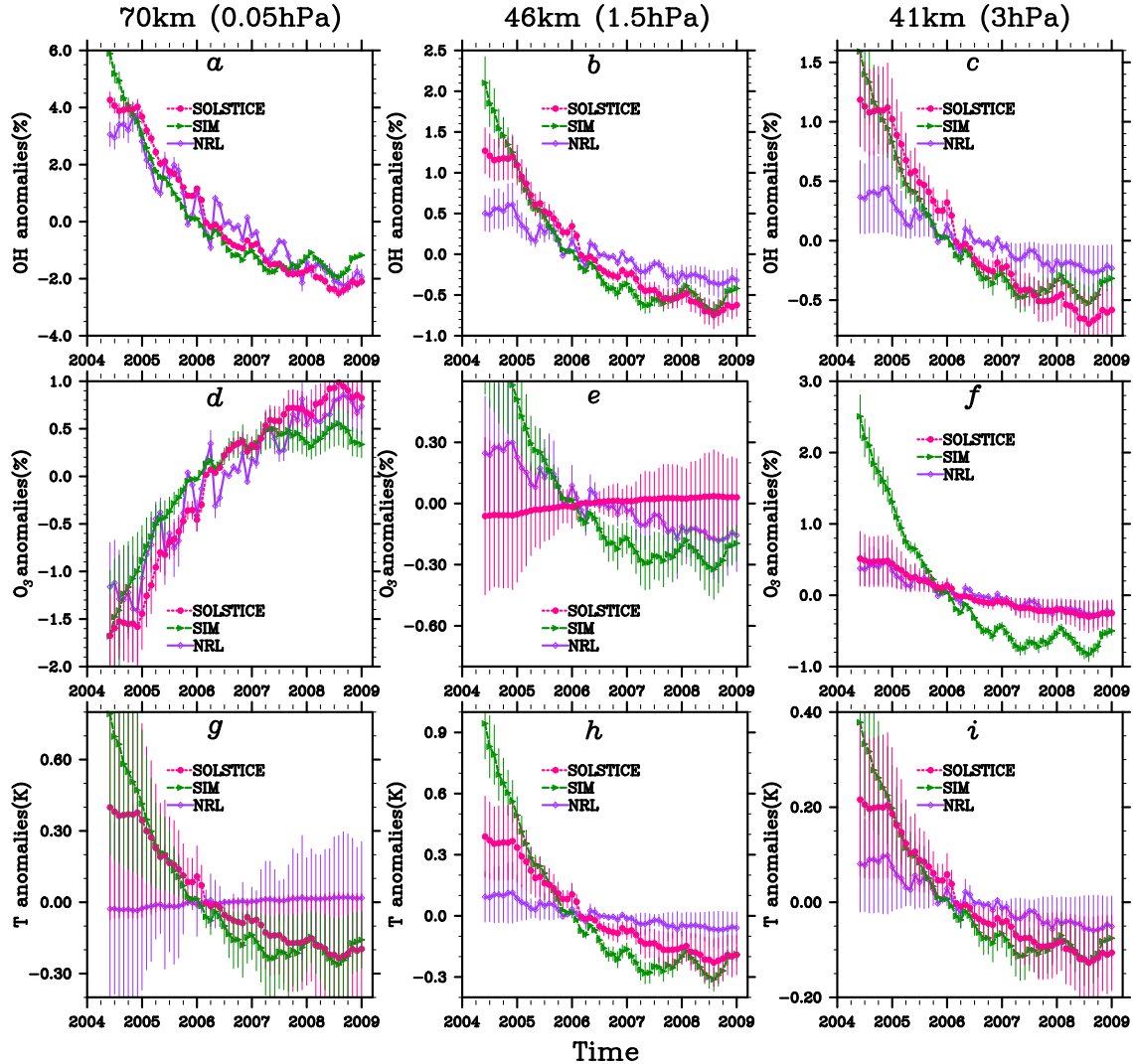


**Figure 4.** The (left) OH, (middle) O<sub>3</sub>, and (right) temperature solar signatures calculated with SIM, SOLSTICE, and NRL data at about (a, d, g) 70 km, (b, e, h) 45 km, and (c, f, i) 40 km. The error bars correspond to 1 $\sigma$  deviations.

agreement. The differences between the 1-D and 3-D responses can be attributed to the dynamics presented in the 3-D model (e.g., changes in Brewer-Dobson circulation can affect the O<sub>3</sub> and temperature responses).

## 5. Comparison With Atmospheric Measurements

[38] The OH, O<sub>3</sub>, and temperature observations used for the comparison were described in section 2.2. The solar signatures discussed in section 4.2 cannot be used for the comparison due to the absence of the NO SUN observed atmospheric time series that would be necessary for the regression model. Therefore, we analyze the tropical mean (18°S–18°N) OH, O<sub>3</sub>, and temperature percentage differences between the data obtained during the periods of the high and low solar activities for all data sets. The differences are calculated for both simulated and observed data. For the comparison of the modeled and simulated differences in the similar dynamical states, we consider the periods corresponding to the same QBO phases. In this study, we compare the modeled and observed responses.

Although the modeled time series are available from May 2004, August 2004 is better covered by atmospheric measurements. Thus, in this section, we study the differences between OH, O<sub>3</sub>, and temperature calculated in August 2004 and August 2008 as these two periods correspond to the same QBO phase, as well as the differences between O<sub>3</sub> obtained in July 2004 and July 2008.

[39] As the modeled time series are calculated as the ensemble of five transient runs, we can estimate the statistical significance of the atmospheric changes between August (July) 2004 and August (July) 2008 using the Student’s two-tailed *t* test. The analysis is performed to find the areas in latitude-altitude space where the NO SUN response is not significant, while the response obtained with the other SSI data sets shows significance of more than 0.95. It would mean that there is a significant atmospheric response to the solar variability in that area. At the same time, there is no significant difference between the dynamical states of the atmosphere corresponding to August (July) 2004 and August (July) 2008. We name it the “Solar significant” case.

[40] The significance of the OH differences between August 2004 and August 2008 is presented in Figures 5a–5d. One can see that the “Solar significant” case can be found at 55–70 km for the OH differences calculated with all SSI data sets and at 40–45 km for the OH differences obtained with the SIM and SOLSTICE data. Then we calculated  $1\sigma$  deviations for the OH difference means to estimate the scattering within the ensemble members obtained with the 3-D model SOCOL (Figure 5e). At 55–70 and 40–45 km, the NO SUN OH change is significantly different from the OH change calculated with other SSI data sets. At 55–70, the difference between the NRL OH change and the OH changes obtained with the SIM and SOLSTICE data is more than  $1\sigma$ , while the discrepancy between the SIM and SOLSTICE OH changes is not significant. The photochemical reasons of the difference between the responses obtained with different SSI at these heights were broadly discussed in section 3.2. The patterns of the OH changes calculated with the 1-D (Figure 2a) and 3-D models are similar, while the values of the 3-D changes are slightly higher. This can be explained by the mismatch of the time points used for the 1-D and 3-D modeling or by the influence of the dynamics (e.g.,

Brewer-Dobson circulation) presented in the 3-D model on the results. The comparison of the 3-D OH modeled changes with the MLS OH changes between August 2004 and August 2008 is presented in Figure 5f. The vertical profile of the OH changes obtained with the MLS data is noisy at 55–70 km. This renders the comparison of the modeled and observed OH changes at these heights impossible. At 43–45 km, the MLS OH changes are close to the SIM and SOLSTICE OH changes.

[41] Figures 6a–6d illustrate the statistical significance of the  $O_3$  differences between August 2004 and August 2008. The tropical areas at 35–45 and 65–80 km correspond to the “Solar significant” conditions. However, as 80 km is the last and, therefore, less trustable SOCOL layer, we will consider the differences at 65–70 km. Figure 6e shows  $1\sigma$  deviations of the  $O_3$  changes calculated with the 3-D SOCOL model. At 35–45 km, only the difference between the SIM and NO SUN  $O_3$  changes can be qualified as significant, while at 65–70 km, the NO SUN  $O_3$  change is different from the  $O_3$  changes calculated with all other data sets. The  $O_3$  changes calculated with the 3-D model are slightly larger than the  $O_3$  responses calculated with the

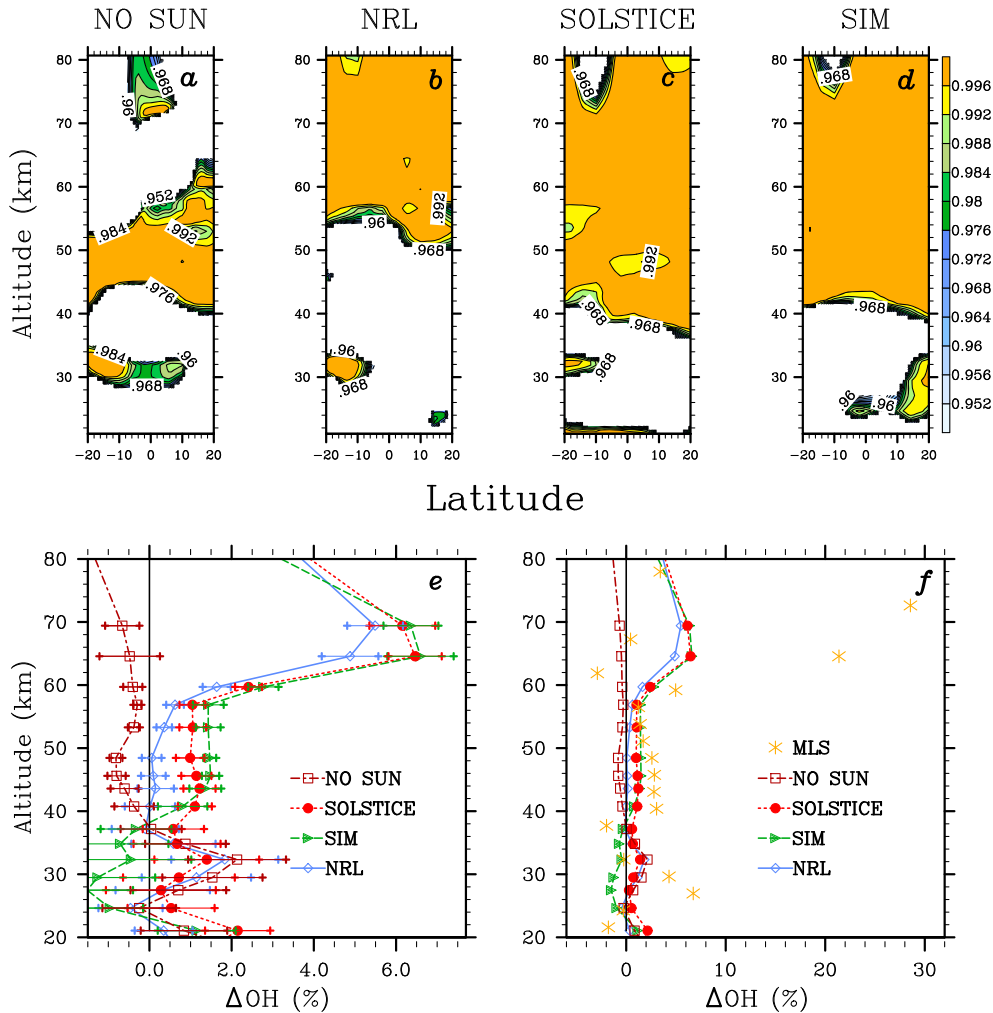


**Figure 5.** The statistical significance of the OH changes between August 2004 and August 2008 calculated for the (a) NO SUN, (b) NRL, (c) SOLSTICE and (d) SIM data. (e) The  $1\sigma$  deviations obtained for the modeled OH changes. (f) Comparison of the modeled OH changes with the MLS OH changes.

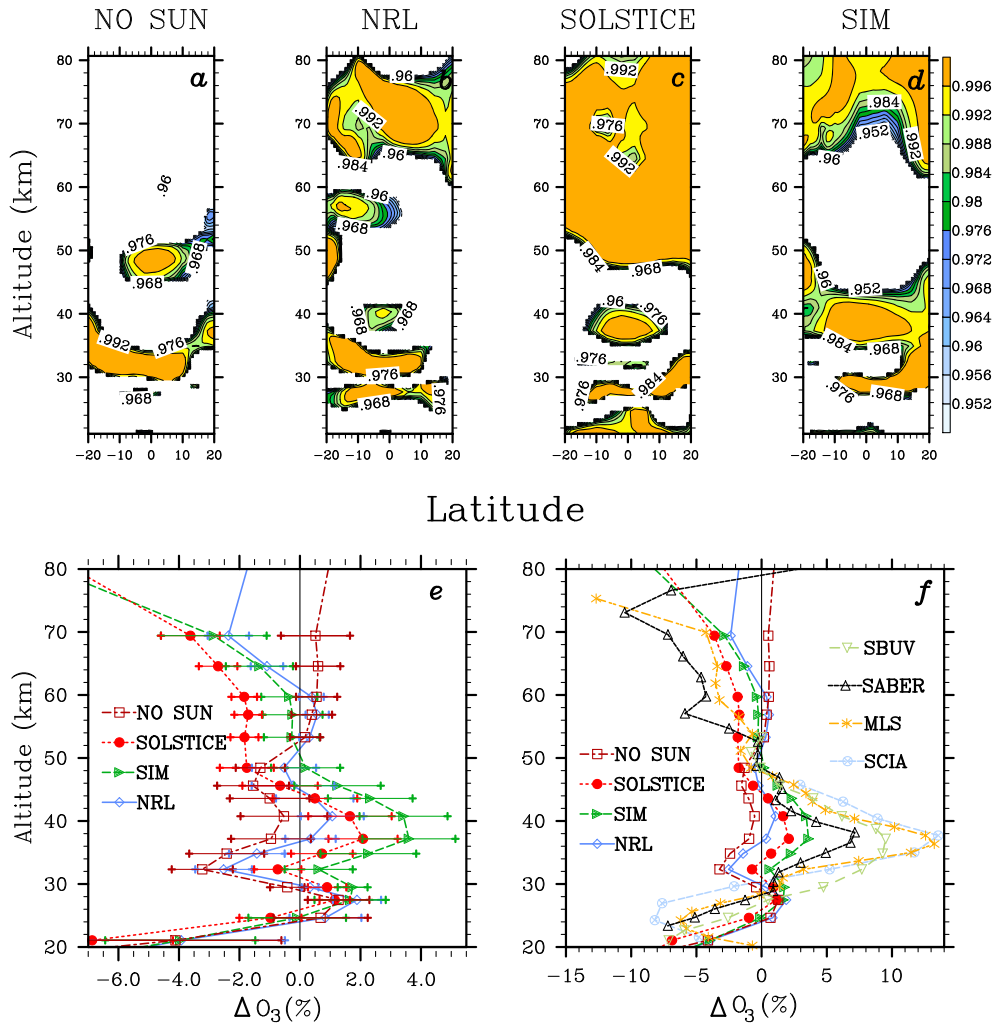


**Figure 6.** The statistical significance of the O<sub>3</sub> changes between August 2004 and August 2008 calculated for the (a) NO SUN, (b) NRL, (c) SOLSTICE, and (d) SIM data. (e) The 1 $\sigma$  deviations obtained for the modeled O<sub>3</sub> changes. (f) The comparison of the modeled O<sub>3</sub> changes with the SBUV, SABER, MLS, and SCIAMACHY O<sub>3</sub> changes.

1-D model at 35–45 km (Figure 2b), while at 45–70 km, the 3-D-modeled O<sub>3</sub> changes are similar to the 1-D O<sub>3</sub> responses. The comparison of the obtained results with observations is shown in Figure 6f. The SABER O<sub>3</sub> changes coincide with the SIM-, SOLSTICE-, and NRL-modeled O<sub>3</sub> changes at 40–45 km, while the O<sub>3</sub> changes obtained with other observations are larger than the modeled changes but can be qualified as similar to the SIM O<sub>3</sub> changes. The O<sub>3</sub> changes calculated from the observations are substantially larger than the modeled O<sub>3</sub> changes at 35–40 km. This difference can be due to some atmospheric processes, which happen in this period of time and are not taken into account by the model. At 65–70 km, the difference between the O<sub>3</sub> changes modeled with the SIM and SOLSTICE SSI and observed by MLS is less than the 1 $\sigma$ . The SABER O<sub>3</sub> changes are smaller than the O<sub>3</sub> modeled changes at these heights. The SABER O<sub>3</sub> changes are closer to the O<sub>3</sub> changes calculated with the SIM and SOLSTICE SSI. The O<sub>3</sub> changes at about 70 km are in good agreement with the results obtained by *Merkel et al.* [2011] for daytime data.

[42] The statistical significance of the temperature differences between August 2004 and August 2008 is shown in Figures 7a–7d. The tropical areas at 35–40 and 50–55 km can be qualified as the “Solar significant” case for all considered data sets. The SIM and SOLSTICE temperature changes are also significant at 70 km. The SOLSTICE temperature changes are significant at 55–70 km. The modeled temperature changes with 1 $\sigma$  deviations are presented in Figure 7e. At about 53–55 km, 1 $\sigma$  difference is found between the NO SUN temperature changes and the changes calculated with the SOLSTICE and SIM SSI, as well as between the SOLSTICE and NRL temperature changes. The SOLSTICE temperature changes are different from the NO SUN and NRL changes at 55–70 km. If we take into account the 1 $\sigma$  deviations, the temperature changes calculated with the 3-D model at about 53–55 km can be qualified as similar to the 1-D results (Figure 2c). At 70 km, there is no any difference between the SIM and SOLSTICE temperature changes, while the 1 $\sigma$  difference can be found between the NO SUN and SOLSTICE temperature changes. The comparison of the modeled changes with the temperature data is shown in Figure 7f. At 70 km,

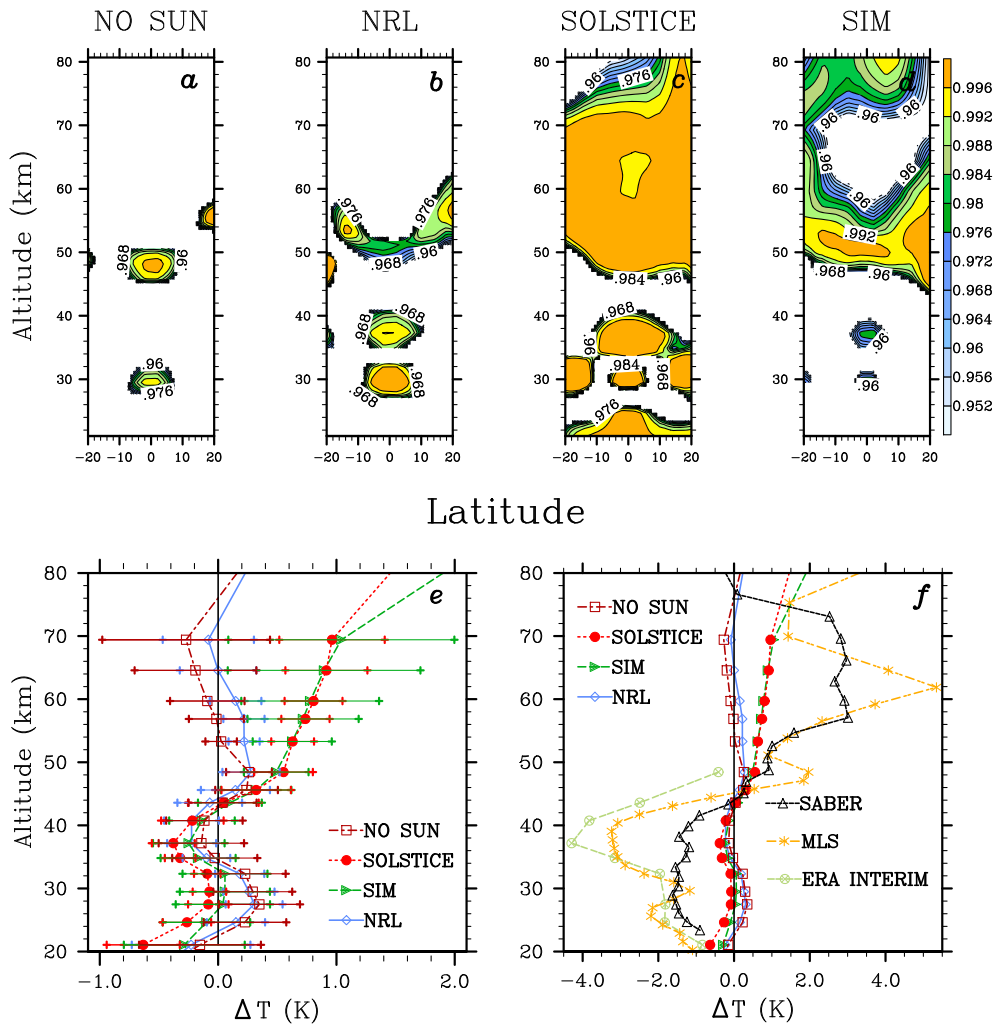


**Figure 7.** The statistical significance of the temperature changes between August 2004 and August 2008 calculated for the (a) NO SUN, (b) NRL, (c) SOLSTICE, and (d) SIM data. (e) The 1 $\sigma$  deviations obtained for the modeled temperature changes. (f) The comparison of the modeled temperature changes with the SABER, MLS, and ERA INTERIM temperature changes.

both MLS temperature changes are close to the modeled temperature changes calculated with the SIM and SOLSTICE SSI, while SABER temperature changes are slightly larger than the SIM changes. At 55–70 km, the SABER and MLS changes are larger than the changes calculated with the SOLSTICE SSI. The SABER and MLS changes are close to the modeled temperature changes calculated with the SIM and SOLSTICE SSI at 53–55 km. At 35–40 km, the modeled temperature changes obtained with the different SSI are similar between each other. Then we could not define the SSI data set that shows the best agreement between observed and modeled responses, which is the main aim of this work. Then the comparison of the temperature results obtained with the model and observations at these heights is not important. However, it is interesting to notice that the temperature changes obtained from the observed data are larger than the changes calculated with the SOCOL model at these heights. The O<sub>3</sub> changes show similar behavior: the changes obtained from the observations are larger than the changes calculated with the model. To estimate the temporal evolution of the O<sub>3</sub> and temperature differences at about 38 km, we calculate these

differences between all months of 2004 and all months of 2008 correspondingly (Figure 8). One can see that the O<sub>3</sub> and temperature differences calculated between Augusts are outliers. All O<sub>3</sub> differences obtained from the observations in August are substantially stronger than the modeled O<sub>3</sub> differences (Figure 8, top). The ERA INTERIM and MLS temperature differences between Augusts (Figure 8, bottom) are substantially smaller than the differences obtained between other months. The SABER data are averaged over 2 months (August and September), which could be the reason why the considered O<sub>3</sub> differences increase and temperature differences decrease are weaker in these data. The O<sub>3</sub> and temperature changes between the high and low solar activity periods calculated with the 3-D SOCOL model are not substantially different from the changes obtained with other most known CCM [Ermolli *et al.*, 2012]. Thus, we can conclude that this discrepancy between the O<sub>3</sub> and temperature August changes obtained with the model and observations are due to some process, which is not taken into account by climate modeling.

[43] Additionally, we consider the O<sub>3</sub> differences between July 2004 and July 2008 to compare the modeled and observed

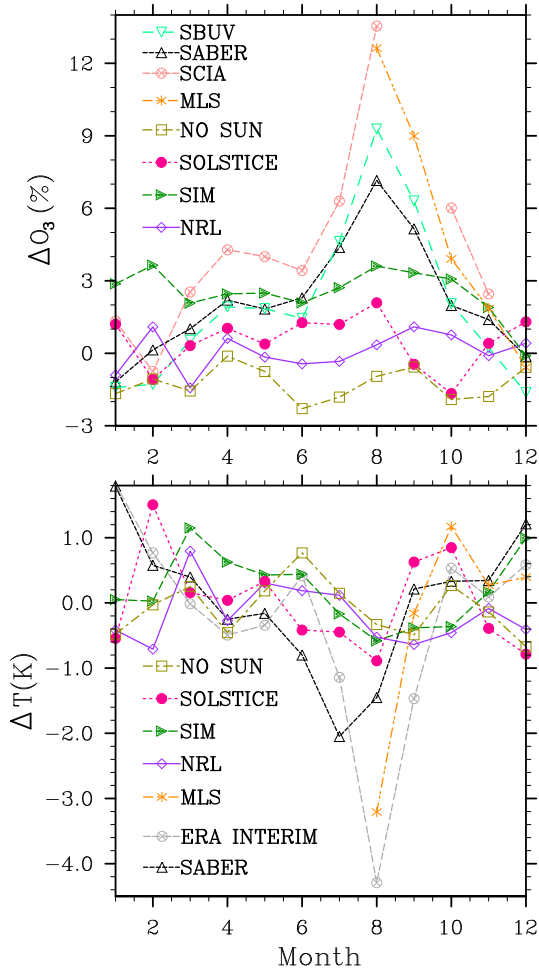


**Figure 8.** The dependency of the (top) ozone and (bottom) temperature differences on months at about 38 km. The value for the month  $X$  corresponds to the difference  $X$ , 2004 –  $X$ , 2008.

results at 35–40 km. The statistical significance of the  $O_3$  differences is shown in Figures 9a–9d. The “Solar significant” case can be found in the tropics at about 36–42 km for the changes calculated with the SIM and SOLSTICE SSI. In Figure 9e, we show the calculated  $O_3$  changes with  $1\sigma$  deviations. One can see that the significant difference can be found between the NO SUN and SIM  $O_3$  changes at about 37 km. The SIM and SOLSTICE  $O_3$  changes at 36–42 km are similar. The comparison of the modeled  $O_3$  changes with observations is presented in Figure 9 f. At 37 km, the SABER  $O_3$  changes (averaged over June and July) coincide with the SIM and SOLSTICE  $O_3$  changes. The SCIA and SBUV  $O_3$  changes at this height are stronger than the  $O_3$  changes calculated with the model but can be qualified as similar to the SIM  $O_3$  changes. Our results and the results obtained by *Merkel et al.* [2011] for the daytime  $O_3$  changes are in good agreement at 37 km.

## 6. Conclusions

[44] We analyze the OH,  $O_3$ , and temperature evolution in the middle atmosphere from May 2004 to February 2009. We apply the 1-D RCMC and 3-D SOCOL models to

calculate the changes with the different SSI data sets. The simulations with the 1-D model allow us to estimate the atmospheric heights where one can expect the strongest discrepancy between the OH,  $O_3$ , and temperature responses to different SSI.

[45] We simulate the OH,  $O_3$ , and temperature solar signatures using the 3-D SOCOL model. We find that the 1-D and 3-D simulated responses overall are in agreement, although at some heights, there are some divergences.

[46] We compare the OH,  $O_3$ , and temperature changes between August 2004 and August 2008 modeled with the different SSI. The comparison is made at the heights where the changes are statistically significant. Then we compare the modeled and observed changes with the purpose to find the SSI data set, which gives the best agreement with the atmospheric measurements. The comparison shows the following.

1. The NO SUN OH changes are different from the changes obtained with the other SSI data sets at 40–45 and 55–70 km. The NRL OH changes are different from the SIM and SOLSTICE OH changes at 55–70 km. The comparison with the measurements shows that the MLS OH changes are similar to the OH changes modeled with the SIM and SOLSTICE data at 43–45 km.
2. The NO SUN  $O_3$  changes are different from the  $O_3$  changes obtained with other SSI at 65–70 km. At 35–45 km, the NO SUN and SIM  $O_3$  changes are different. The comparison with the atmospheric measurements shows that the MLS  $O_3$  changes are similar to the SIM and SOLSTICE  $O_3$  changes at 65–70 km. At 40–45 km, the SABER  $O_3$  changes and the  $O_3$  changes simulated with NRL, SIM, and SOLSTICE SSI are comparable.
3. The NO SUN temperature changes are different from the temperature changes calculated with SIM and SOLSTICE SSI at 53–55 km. At these heights, the NRL and SOLSTICE temperature changes are also distinguishable. At 70 km, there is a difference between the temperature changes modeled with the NO SUN and SOLSTICE data. The comparison with the atmospheric measurements shows that the MLS temperature changes are similar to the changes calculated with the SIM and SOLSTICE data at 70 km. At 53–55 km, the SABER and MLS temperature changes and the changes modeled with the SIM and SOLSTICE data are comparable.

[47] At 35–40 km, the  $O_3$  changes obtained from the observations are substantially larger than the modeled changes. The  $O_3$  changes calculated between other months of 2004 and 2008 do not show such behavior. Therefore, for the comparison of the  $O_3$  modeled changes with observations at 35–40 km, we analyze the  $O_3$  differences calculated between July 2004 and July 2008. The NO SUN and SIM  $O_3$  changes are different at 37 km. The SABER  $O_3$  changes obtained between July 2004 and July 2008 at about 37 km are similar to the SIM and SOLSTICE  $O_3$  changes.

[48] Thus, our analysis shows that in the most of cases, the observed OH,  $O_3$ , and temperature changes are in reasonable agreement with the changes modeled with the SIM and SOLSTICE SSI.

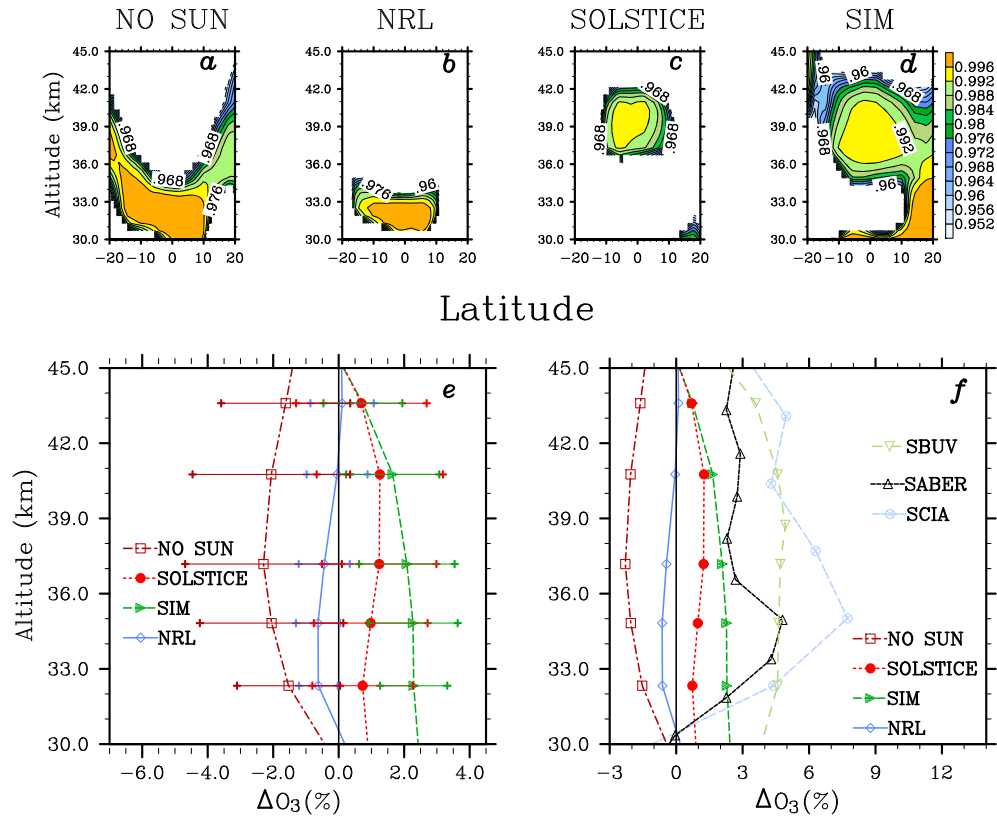


**Figure 9.** The statistical significance of the O<sub>3</sub> changes between July 2004 and July 2008 calculated for the (a) NO SUN, (b) NRL, (c) SOLSTICE, and (d) SIM data. (e) The 1 $\sigma$  deviations obtained for the modeled O<sub>3</sub> changes. (f) The comparison of the modeled O<sub>3</sub> changes with the SBUV, SABER, and SCIAMACHY O<sub>3</sub> changes.

[49] **Acknowledgments.** This research was funded in part by the Swiss National Science Foundation under grant agreements 200020 130102, 200020 140573, and CRS1122-130642 (FUPSOL) and in part by the European Community's Seventh Framework Programme (FP7/2007-2013) under grant agreement 218816 (SOTERIA). This work was supported in part by COST Action ES1005 TOSCA (<http://www.tosca-cost.eu>). We would like to thank the MLS/AURA, SBUV, and ERA INTERIM science teams for their work in producing the data sets used in this paper. The National Center for Atmospheric Research is sponsored by the National Science Foundation. We would also like to thank IUP Bremen for providing us data.

## References

- Bovensmann, H., J. P. Burrows, M. Buchwitz, J. Frerick, S. Noël, V. V. Rozanov, K. V. Chance, and A. P. H. Goede (1999), SCIAMACHY: Mission objectives and measurement modes, *J. Atmos. Sci.*, *56*, 127–150.
- Brasseur, G. (1993), The response of the middle atmosphere to long-term and short-term solar variability: A two-dimensional model, *J. Geophys. Res.*, *98*(D12), 23079–23090, doi:10.1029/93JD02406.
- Brasseur, G., and S. Solomon (2005), *Aeronomy of the Middle Atmosphere: Chemistry and Physics of the Stratosphere and Mesosphere*, 3rd ed., Springer, Dordrecht, Netherlands.
- Brueckner, G. E., K. L. Edlow, L. E. Floyd IV, J. L. Lean, and M. E. VanHoosier (1993), The Solar Ultraviolet Spectral Irradiance Monitor (SUSIM) Experiment on board the Upper Atmosphere Research Satellite (UARS), *J. Geophys. Res.*, *98*(D6), 10695–10711, doi:10.1029/93JD00410.
- Burrows, J. P., E. Holzle, A. P. H. Goede, H. Visser, and W. Fncke (1995), SCIAMACHY—Scanning Imaging Absorption Spectrometer for Atmospheric Cartography, *Acta Astronaut.*, *35*(7), 445–451.
- Cahalan, R. F., G. Wen, J. W. Harder, and P. Pilewskie (2010), Temperature responses to spectral solar variability on decadal time scales, *Geophys. Res. Lett.*, *37*, L07705, doi:10.1029/2009GL041898.
- Dee, D. P., et al. (2011), The ERA-Interim reanalysis: Configuration and performance of the data assimilation system, *Q. J. R. Meteorol. Soc.*, *137*, 553–597, doi:10.1002/qj.828.
- Egorova, T., I. Karol, and E. Rozanov (1997), The influence of ozone content loss in the lower stratosphere on the radiative balance of the troposphere, *Phys. Atmos. Ocean (Russ. Acad. Sci.)*, *33*, 492–499.
- Egorova, T. A., E. V. Rozanov, V. A. Zubov, and I. L. Karol (2003), Model for Investigating Ozone Trends (MEZON), *Phys. Atmos. Ocean (Russ. Acad. Sci.)*, *39*(N3), 277–292.
- Egorova, T., E. Rozanov, V. Zubov, E. Manzini, W. Schmutz, and T. Peter (2005), Chemistry-climate model SOCOL: A validation present-day climatology, *Atmos. Chem. Phys.*, *5*, 1557–1576, SRef-ID: 1680-7324/acp/2005-5-1557.
- Ermolli, I., et al. (2012), Recent variability of the solar spectral irradiance and its impact on climate modeling, *Atmos. Chem. Phys. Disc.*, *12*(9), 24557–24642.
- Fleming, E. L., S. Chandra, C. H. Jackman, D. B. Considine, and A. R. Douglass (1995), The middle atmosphere response to short and long term UV variations: An analysis of observations and 2D model results, *J. Atmos. Terr. Phys.*, *57*, 333–365.
- Fomichev, V. L., J.-P. Blanchet, and D. S. Turner (1998), Matrix parameterization of the 15  $\mu$ m CO<sub>2</sub> band cooling in the middle and upper atmosphere for variable CO<sub>2</sub> concentration, *J. Geophys. Res.*, *103*(D10), 11505–11528, doi:10.1029/98JD00799.
- Giorgetta, M. A. (1996), Der Einfluss der quasi-zweijährigen Oszillation: Modellrechnungen mit ECHAM4, Max-Planck-Institut für Meteorologie, Hamburg, Examensarbeit Nr. 40, MPI-Report218.
- Haigh, J. D., A. R. Winning, R. Toumi, and J. W. Harder (2010), An influence of solar spectral variations on radiative forcing of climate, *Nature*, *467*, 696–699, doi:10.1038/nature09426.
- Harder, J., G. M. Lawrence, G. Rottman, and T. Woods (2000), Solar Spectral Irradiance Monitor (SIM), *Metrologia*, *37*, 415–418.
- Harder, J., J. Fontenla, G. Lawrence, T. Woods, and G. Rottman (2005a), The Spectral Irradiance Monitor: Measurements Equations and Calibration, *Solar Phys.*, *220*(1–2), 169–204, doi:10.1007/s11207-005-1528-1.
- Harder, J., G. Lawrence, J. Fontenla, G. Rottman, and T. Woods (2005b), The Spectral Irradiance Monitor: Scientific Requirements, Instrument

- Design, and Operation Modes, *Solar Phys.*, 230(1–2), 141–167, doi:10.1007/s11207-005-5007-5.
- Harder, J. W., J. M. Fontenla, P. Pilewskie, E. C. Richard, and T. N. Woods (2009), Trends in solar spectral irradiance variability in the visible and infrared, *Geophys. Res. Lett.*, 36, L07801, doi:10.1029/2008GL036797.
- Heath, D. F., A. J. Krueger, H. R. Roeder, and B. D. Henderson (1975), The solar backscatter ultraviolet and total ozone mapping spectrometer (SBUV/TOMS) for Nimbus G, *Opt. Eng.*, 14, 323–331.
- Kazil, J. (2002), The University of Bern atmospheric ion model: Time-dependent ion modeling in the stratosphere, mesosphere and lower thermosphere, PhD thesis, Univ. of Bern, Switzerland.
- Kopp, E. (1996), Electron and ion densities, in *The Upper Atmosphere: Data Analysis and Interpretation*, edited by W. Dieminger, G. Hartmann, and R. Leitinger, pp. 625–635, Springer Verlag, New York.
- Krivova, N. A., S. K. Solanki, T. Wenzler, and B. Podlipnik (2009), Reconstruction of solar UV irradiance since 1974, *J. Geophys. Res.*, 114, D00I04, doi:10.1029/2009JD012375.
- Lean, J. L. (1997), The Sun's variable radiation and its relevance for Earth, *Annu. Rev. Astron. Astrophys.*, 35, 33–67, doi:10.1146/annurev.astro.35.1.33.
- Lean, J. L. (2000), Evolution of the Sun's spectral irradiance since the Maunder minimum, *Geophys. Res. Lett.*, 27, 2425–2428, doi:10.1029/2000GL000043.
- Lean, J., G. Rottman, J. Harder, and G. Kopp (2005), SORCE contributions to new understanding of global change and solar variability, *Solar Phys.*, 230, 27–53.
- Livesey, N., et al. (2011), Version 3.3 Level 2 data quality and description document, JPL D-33509.
- Manzini, E., and L. Bengtsson (1996), Stratospheric climate and variability from a general circulation model and observations, *Clim. Dyn.*, 12, 615–639.
- McClintock, W. E., M. Snow, and T. N. Woods (2005), Solar Stellar Irradiance Comparison Experiment II (SOLSTICE II): Pre-launch and on-orbit calibrations, *Sol. Phys.*, 230, 259–294.
- Merkel, A. W., J. W. Harder, D. R. Marsh, A. K. Smith, J. M. Fontenla, and T. N. Woods (2011), The impact of solar spectral irradiance variability on middle atmospheric ozone, *Geophys. Res. Lett.*, 38, L13802, doi:10.1029/2011GL047561.
- Oberländer, S., U. Langematz, K. Matthes, M. Kunze, A. Kubin, J. Harder, N. A. Krivova, S. K. Solanki, J. Paganan, and M. Weber (2012), The influence of spectral solar irradiance data on stratospheric heating rates during the 11 year solar cycle, *Geophys. Res. Lett.*, 39, L01801, doi:10.1029/2011GL049539.
- Ozolin, Y., I. Karol, E. Rozanov, and T. Egorova (2009), Ion chemistry in the D-layer of the ionosphere and the 1-D modeling of the solar proton event effects on the ion and gas composition of the mesosphere 4, *Izv. Atmos. Ocean. Phys.*, 5(6), 737–750.
- Paganan, J., M. Weber, M. T. DeLand, L. E. Floyd, and J. P. Burrows (2011), Solar spectral irradiance variations in 240–1600 nm during the recent solar cycles 21–23, *Solar Phys.*, 272(1), 159–188, doi:10.1007/s11207-011-9808-4.
- Rayner, N. A., D. E. Parker, E. B. Horton, C. K. Folland, L. V. Alexander, D. P. Rowell, E. C. Kent, and A. Kaplan (2003), Global analyses of sea surface temperature, sea ice, and night marine air temperature since the late nineteenth century, *J. Geophys. Res.*, 108, 4407, doi:10.1029/2002JD002670.
- Rottman, G. J., T. N. Woods, and T. P. Sparr (1993), Solar-Stellar Irradiance Comparison Experiment 1: 1. Instrument design and operation, *J. Geophys. Res.*, 98(D6), 10667–10677, doi:10.1029/93JD00462.
- Rottman, G., J. Harder, J. Fontenla, T. N. Woods, O. R. White, and G. Lawrence (2005), The Spectral Irradiance Monitor (SIM): Early observations, *Sol. Phys.*, 230, 205.
- Rozanov, E., V. Zubov, M. Schlesinger, F. Yang, and N. Andronova (1999), The UIUC three-dimensional stratospheric chemical transport model: Description and evaluation of the simulated source gases and ozone, *J. Geophys. Res.*, 104, 11755–11782.
- Rozanov, E. V., M. E. Schlesinger, and V. A. Zubov (2001), The University of Illinois, Urbana-Champaign three-dimensional stratosphere-troposphere general circulation model with interactive ozone photochemistry: Fifteen-year control run climatology, *J. Geophys. Res.*, 106(D21), 27,233–27,254, doi:10.1029/2000JD000058.
- Rozanov, E., T. Egorova, C. Fröhlich, M. Haberleiter, T. Peter, and W. Schmutz (2002), Estimation of the ozone and temperature sensitivity to the variation of spectral solar flux, in *From Solar Min to Max: Half a Solar Cycle With SOHO*, ESA SP-508, pp. 181–184.
- Rozanov, E., T. Egorova, W. Schmutz, and T. Peter (2006), Simulation of the stratospheric ozone and temperature response to the solar irradiance 521 variability during Sun rotation cycle, *J. Atmos. Sol. Terr. Phys.*, 68(522) 2203–2213.
- Russell, J. M., III, M. G. Mlynczak, L. L. Gordley, J. Tansock, and R. Esplin (1999), An overview of the SABER experiment and preliminary calibration results, *Proc. SPIE Int. Soc. Opt. Eng.*, 3756, 277–288.
- Sander, S. P., et al. (2006), Chemical Kinetics and Photochemical Data for Use in Atmospheric Studies. Evaluation Number 15, JPL Publication 06-2, Jet Propulsion Laboratory, Pasadena.
- Shapiro, A. I., W. Schmutz, E. Rozanov, M. Schoell, M. Haberleiter, A. V. Shapiro, and S. Nyeki (2011a), A new approach to the long-term reconstruction of the solar irradiance leads to large historical solar forcing, *Astron. Astrophys.*, 529, A67, doi:10.1051/0004-6361/201016173.
- Shapiro, A. V., E. Rozanov, T. Egorova, A. I. Shapiro, T. Peter, and W. Schmutz (2011b), Sensitivity of the Earth's middle atmosphere to short-term solar variability and its dependence on the choice of solar irradiance data set, *J. Atmos. Sol. Terr. Phys.*, 73, 348–355.
- Shapiro, A. V., E. Rozanov, A. I. Shapiro, S. Wang, T. Egorova, W. Schmutz, and T. Peter (2012), Signature of the 27-day solar rotation cycle in mesospheric OH and H<sub>2</sub>O observed by the Aura Microwave Limb Sounder, *Atmos. Chem. Phys.*, 12, 3181–3188, doi:10.5194/acp-12-3181-2012.
- Smith, A. K., and K. Matthes (2008), Decadal-scale periodicities in the stratosphere associated with the solar cycle and the QBO, *J. Geophys. Res.*, 113, D05311, doi:10.1029/2007JD009051.
- Solanki, S. K., and Y. C. Unruh (1998), A model of the wavelength dependence of solar irradiance variations, *Astron. Astrophys.*, 329, 747–753.
- Swartz W. H., R. S. Stolarski, L. D. Oman, E. L. Fleming, and C. H. Jackman (2012), Middle atmosphere response to different descriptions of the 11-yr solar cycle in spectral irradiance in a chemistry-climate model, *Atmos. Chem. Phys. Disc.*, 12(3), 7039–7071.
- Thuillier, G., et al. (2003), The solar spectral irradiance from 200 to 2400 nm as measured by the SOLSPEC spectrometer from the ATLAS and EURECA missions, *Solar Phys.*, 214, 1–22.
- Tsutsui, J., K. Nishizawa, and F. Sassi (2009), Response of the middle atmosphere to the 11-year solar cycle simulated with the whole atmosphere community climate model, *J. Geophys. Res.*, 114, D02111.
- Waters, J. W., et al. (2006), The Earth Observing System Microwave Limb Sounder (EOS MLS) on the Aura Satellite, *IEEE Trans. Geosci. Remote Sens.*, 44(5), 1075–1092, doi:10.1109/TGRS.2006.873771.